International Journal of Multiphase Flow 193 (2025) 105387

Contents lists available at ScienceDirect

International Journal of Multiphase Flow

journal homepage: www.elsevier.com/locate/ijmulflow

Research Paper

Droplet impact and splashing on surfactant-laden shallow pools

Miguel A. Quetzeri-Santiago [a,*], C. Ricardo Constante-Amores [b], Thomas C. Sykes [c,d], Seungwon Shin [e], Jalel Chergui [f], Damir Juric [f,g], J. Rafael Castrejón-Pita [h], Alfonso A. Castrejón-Pita [d]

[a] Instituto de Investigaciones en Materiales, Universidad Nacional Autónoma de México, Cd. Universitaria, 04510 Mexico City, Mexico
[b] Department of Mechanical Science and Engineering, University of Illinois, Urbana Champaign, IL 61801, USA
[c] School of Engineering, University of Warwick, Coventry CV4 7AL, United Kingdom
[d] Department of Engineering Science, University of Oxford, Oxford OX1 3PJ, United Kingdom
[e] Department of Mechanical and System Design Engineering, Hongik University, Republic of Korea
[f] Université Paris Saclay, Centre National de la Recherche Scientifique (CNRS), Laboratoire Interdisciplinaire des Sciences du Numérique (LISN), 91400 Orsay, France
[g] Department of Applied Mathematics and Theoretical Physics, University of Cambridge, Cambridge CB3 0WA, United Kingdom
[h] Department of Mechanical Engineering, University College London, Torrington Place, London, WC1E 7JE, United Kingdom

ARTICLE INFO

Keywords:
Droplet impact
Shallow pools
Surfactants
Splashing
Dynamic surface tension

ABSTRACT

From inkjet printing to agricultural spraying, the impact of droplets onto complex-fluid pools plays a crucial role in various fields. To reveal the effects that surfactants play in the dynamics of splashing, we combine high-speed imaging and 3D numerical simulations allowing us to investigate crown formation and breakup when a clean droplet strikes a surfactant-laden pool. We first characterise three surfactants (Surfynol 465, SDS, and Triton X-100) by measuring their dynamic surface tension, in relation to the characteristic crown-collapse time, t_c. High-speed imaging reveals three distinct post-impact regimes (smooth receding, recoiling breakup, and splashing), based on the Weber number, where 'fast-acting' surfactants trigger splashing at significantly lower Weber numbers than 'slow-acting' or surfactant-free systems. To probe the smooth-receding regime in detail, we developed and experimentally-validated numerical simulations for SDS-laden pools, capturing both reduced surface tension and Marangoni stresses. Varying the Peclet number reveals that surfactant transport slows crown evolution, producing taller, narrower sheets with approximately 5% more interfacial area but lower kinetic energy than in the clean case. Our results demonstrate that the dynamic surface tension at t_c serves as a reliable predictor of the onset of splashing, while the Peclet number governs the crown morphology. By elucidating the interplay between surfactant kinetics and fluid inertia, this work offers critical insights for optimising droplet-based technologies, such as coatings, 3D printing, and pesticide applications where precise control over splashing and fragmentation is essential.

1. Introduction

Droplet impact dynamics on liquid surfaces play a critical role in various industrial and scientific applications, including inkjet printing, pesticide spraying, 3D printing, and coatings (Martin et al., 2008; Bergeron et al., 2000; Quetzeri-Santiago et al., 2019; Herczyński et al., 2011). In nature, phenomena such as soil erosion, botanical disease transmission, and stalagmite formation are also influenced by droplet impact dynamics (Cheng et al., 2022; Gilet and Bourouiba, 2015; Parmentier et al., 2019). Understanding droplet behaviour during impacts is essential for controlling and optimising these processes.

The study of droplet-pool impact dates back to the pioneering work of A. M. Worthington and H. E. Edgerton, who used flash photography to capture these events (Worthington, 1908; Edgerton, 1977). In their works, they observed that the impact of a droplet onto a thin liquid layer of the same liquid gives rise to the formation of a vertical lamella, and eventually its fragmentation into a myriad of smaller droplets. Advances in high-speed imaging and computational methods have further propelled this field, allowing researchers to observe details at the micrometer scale and timescales of less than 1 ms (Thoroddsen, 2002; Thoraval et al., 2012; Fudge et al., 2021; Kroeze et al., 2024).

* Corresponding author.
E-mail addresses: mquetzeri@materiales.unam.mx (M.A. Quetzeri-Santiago), crconsta@illinois.edu (C.R. Constante-Amores), r.pita@ucl.ac.uk (J.R. Castrejón-Pita), alfonso.castrejon-pita@eng.ox.ac.uk (A.A. Castrejón-Pita).

https://doi.org/10.1016/j.ijmultiphaseflow.2025.105387
Received 4 June 2025; Received in revised form 21 July 2025; Accepted 31 July 2025
Available online 11 August 2025

Droplet impacts on pools can result in the formation of a Worthington jet as the air cavity trapped below the free surface after the impact collapses, resulting in a vertical jet. A similar phenomenon is also observed in other cases, such as bursting bubbles (Blanchard and Syzdek, 1972; Deike et al., 2018; Jiang et al., 2022). Other studies have examined the effects of varying pool depth on mixing, impact forces, bubble ring entrapment at high Reynolds numbers, and splashing, all of which involve pure liquids (Ersoy and Eslamian, 2020; Yu et al., 2022; Thoraval et al., 2013; Cossali et al., 1997; Sykes et al., 2023). On the other hand, there are only a handful of studies exploring the effects of other additives, for instance leading to viscoelastic behaviour, in the context of high-speed drop impact onto pools and/or films, such as in Singh et al. (2025)

Apart from the pool depth, the impact dynamics on the same liquid are typically characterised by two dimensionless numbers: the Weber number $We = \rho U^2 D/\sigma$ and the Reynolds number $Re = \rho U D/\mu$, where ρ, σ, μ, and D represent the droplet density, surface tension, viscosity, and diameter, respectively, and U is the impact velocity. At high Weber and Reynolds numbers, i.e., $We \gg 1$ and $Re \gg 1$, phenomena such as crown formation, finger formation, and secondary droplet detachment are expected, irrespective of pool depth. However, pool depth significantly influences the evolution of the ejecta sheet and splashing propensity. On shallow pools, the ejecta sheet collects fluid from the pool and transforms into a lamella, while in deeper pools, it remains distinct and folds inward towards the axis of symmetry (Sykes et al., 2023).

Most natural and industrial streams are contaminated with surfactants (i.e. surface-active agents), which may lead to gradients in surface tension, and subsequently induce the formation of Marangoni and surface viscous stresses. The late stages of the droplet-pool impact involve the formation of ligaments, and their eventual breakup to form droplets. Previous research has highlighted the crucial role of surfactants on capillary singularities the increase in Leidenfrost temperature. (Ananthakrishnan and Yeung, 1994; Craster et al., 2002; Liao et al., 2004; Kamat et al., 2018; Constante-Amores et al., 2022; Prasad et al., 2022). Therefore, we might expect that surfactant-induced effects can significantly alter the behaviour of the late stages of the impacting dynamics, influencing phenomena such as splashing, recoiling, and the formation of secondary droplets (Hoffman et al., 2021a; Lohse, 2022; Varghese et al., 2024; Constante-Amores et al., 2023a; Che and Matar, 2017). Che and Matar (2017) studied experimentally the role of surfactants in late-stage droplet impact phenomena, showing significant alterations in post-impact phenomena like capillary wave propagation, crown development, and secondary droplet production. However, Marangoni stresses, surfactant concentration dynamics and type of surfactant were not investigated.

Constante-Amores et al. (2023a) demonstrated that the presence of surfactants significantly alters the later stages of impact, playing a crucial role in the formation of larger ligaments. Surfactant-induced effects reopen the neck, delaying droplet formation. However, they also show that surfactants do not influence wave selection in the rim, leaving the Rayleigh–Plateau instability as the primary mechanism determining the rim wavelength. However, this study did not explore factors such as the Peclet number ($Pe_s = UD/D_s$, where D_s is the interfacial diffusion coefficient), which will define what is called a *slow* and *fast* surfactant (Hoffman et al., 2021b).

This study aims to investigate the impact dynamics of surfactant-free water-glycerol droplets on shallow pools containing various types of surfactant. Through a series of experiments and 3D numerical simulations, we seek to provide a comprehensive understanding of how different surfactants affect droplet impact behaviour.

The paper is organised as follows, Section 2 provides a detailed explanation of the experimental and numerical framework. Section 3 presents the description of the results concerning the distribution of surfactant along the interfaces and a regime map depending on the value of Weber and the gradient of surface tension. Finally, concluding remarks are summarised in Section 4.

2. Methodology

2.1. Experimental details

In this work, we used a water-glycerol mixture (70/30 by volume) with a viscosity of 3.2 ± 0.1 cP, measured with a Hydramotion Viscolite 700. We used this mixture so as to stay in the lamella formation regime for a wide range of Weber numbers (Sykes et al., 2023). This mixture was the base for preparing solutions with three commercially available surfactants: sodium dodecyl sulfate (SDS), Triton X-100 (both purchased from Sigma-Aldrich), and Surfynol 465 (free sample from Evonik). The concentrations used were 2.45 g/L for SDS, 0.15 g/L for Triton X-100, and 10.32 g/L for Surfynol 465 (which is approximately 1 CMC for all the surfactants). To create a surfactant-free liquid with the same viscosity as the other solutions and a similar equilibrium surface tension, we prepared an ethanol and glycerol solution.

The dynamic surface tension was measured using an MBP tensiometer (Sinterface BPA-2S) based on the bubble pressure method. In this technique, air is blown at a controlled flow rate to produce bubbles within the test liquid. The bubble's lifetime – determined by the flow rate – affects the time that surfactant molecules have to adsorb at the bubble's surface. The method implemented by the BPA-2S enables surface lifetimes to be measured in the range of 0.2×10^{-3} to 11.5 s. See Varghese et al. (2024) and Fainerman and Miller (1998) for a detailed description.

Our experiments involved dripping surfactant-free water-glycerol droplets into shallow pools of a surfactant-laden version of the same base fluid. The experimental setup is shown in Fig. 1. Droplets were generated using stainless steel blunt-end dispensing tips, resulting in drop diameters of $D_0 = 2.22 \pm 0.01$ mm. These droplets impacted the shallow pools, which were created by dispensing 3.08 ml of one of the surfactant solutions into a titanium disk with an inner diameter of 70 mm and a depth of 200 μm. The titanium surface was rinsed and dried after each impact to prevent contamination and maintain surfactant concentration. All experiments were conducted at 23 ± 1°C to minimise temperature effects on surfactant properties.

The height of the dispensed needle was varied to obtain velocities ranging from 2.0 to 3.7 ms^{-1}. The impact velocity and drop diameters were measured with an in-house MATLAB code. Droplet impacts were recorded using a shadowgraph configuration with a Phantom v2512 high-speed camera, equipped with a Tamron 90 mm macro lens and illuminated by a 100 W CoB LED. The recording resolution was 1280 x 800, with an exposure time of 10 μs and a frame rate of 25000 frames per second.

2.2. Numerical simulations

High resolution simulations were performed by solving the two-phase incompressible Navier–Stokes equations with surface tension in a three-dimensional Cartesian domain $\mathbf{x} = (x, y, z)$ (see Fig. 1b). The interface between the gas and liquid is described by a hybrid front-tracking/level-set method, where surfactant transport is resolved at the interface (Shin et al., 2018). Here, and in what follows, all variables are made dimensionless (represented by tildes) using

$$\tilde{\mathbf{x}} = \frac{\mathbf{x}}{D_o}, \quad \tilde{t} = \frac{t}{t_r}, \quad \tilde{\mathbf{u}} = \frac{\mathbf{u}}{U}, \quad \tilde{p} = \frac{p}{\rho U^2}, \quad \tilde{\sigma} = \frac{\sigma}{\sigma_s}, \quad \tilde{\Gamma} = \frac{\Gamma}{\Gamma_\infty}, \tag{1}$$

here, t, $\mathbf{u}$, and p represent time, velocity, and pressure, respectively. The physical parameters include the liquid density ρ, liquid viscosity μ, surface tension σ, surfactant-free surface tension σ_s, drop impact velocity U, and initial drop diameter D_o. Consequently, the characteristic time scale is given by $t_r = D_o/U$. The interfacial surfactant concentration Γ is normalised by the saturation interfacial concentration Γ_∞.

As a result of this scaling, the dimensionless equations read

$$\nabla \cdot \tilde{\mathbf{u}} = 0, \tag{2}$$

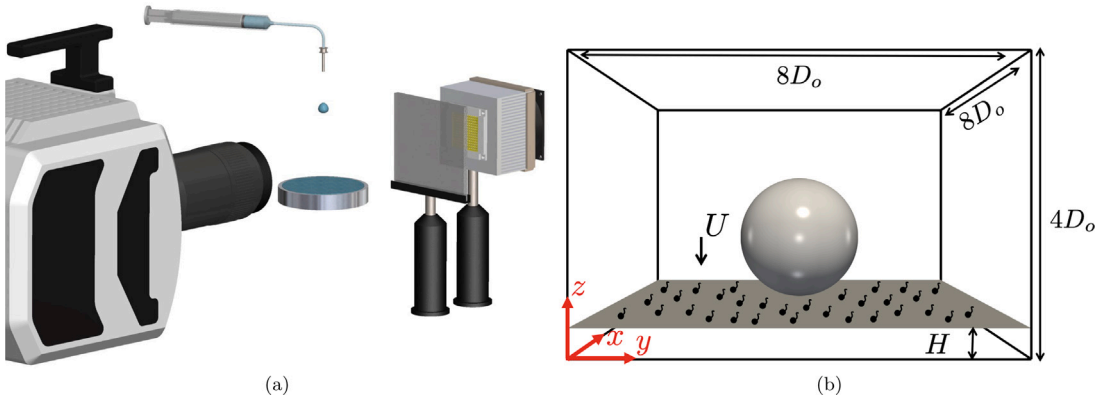

Fig. 1. (a) Schematic view of the experimental setup used to visualise the impact of droplets on the shallow pools. We use a Phantom v2512 high-speed camera equipped with a Tamron macro lens and lighting provided by a 100 W LED, in a shadowgraph configuration. (b) Schematic representation of the initial configuration of the simulation.

$$\tilde{\rho}\left(\frac{\partial \tilde{\mathbf{u}}}{\partial \tilde{t}}+\tilde{\mathbf{u}}\cdot\nabla\tilde{\mathbf{u}}\right)+\nabla\tilde{p}=-\frac{\tilde{\rho}\mathbf{i}_z}{Fr}+\frac{1}{Re}\nabla\cdot\left[\tilde{\mu}(\nabla\tilde{\mathbf{u}}+\nabla\tilde{\mathbf{u}}^T)\right]+$$

$$+\frac{1}{We}\int_{\tilde{A}(\tilde{t})}(\tilde{\sigma}\tilde{\kappa}\mathbf{n}+\nabla_s\tilde{\sigma})\delta\left(\tilde{\mathbf{x}}-\tilde{\mathbf{x}}_f\right)\mathrm{d}\tilde{A}, \tag{3}$$

$$\frac{\partial\tilde{\Gamma}}{\partial\tilde{t}}+\nabla_s\cdot(\tilde{\Gamma}\tilde{\mathbf{u}}_t)=\frac{1}{Pe_s}\nabla_s^2\tilde{\Gamma}, \tag{4}$$

where the density and viscosity are given by $\tilde{\rho}=\rho_g/\rho+\left(1-\rho_g/\rho\right)\mathcal{H}\left(\tilde{\mathbf{x}},\tilde{t}\right)$ and $\tilde{\mu}=\mu_g/\mu+\left(1-\mu_g/\mu\right)\mathcal{H}\left(\tilde{\mathbf{x}},\tilde{t}\right)$ wherein $\mathcal{H}\left(\tilde{\mathbf{x}},\tilde{t}\right)$ represents a Heaviside function, which is zero in the gas phase and unity in the liquid phase, while the subscript 'g' designates the gas phase, and $\tilde{\mathbf{u}}_t=\left(\tilde{\mathbf{u}}_s\cdot\mathbf{t}\right)\mathbf{t}$ is the tangential velocity at the interface in which $\tilde{\mathbf{u}}_s$ represents the interfacial velocity, and κ is the curvature. The interfacial gradient is given by $\nabla_s=(\mathbf{I}-\mathbf{nn})\cdot\nabla$ wherein $\mathbf{I}$ is the identity tensor and $\mathbf{n}$ is the outward-pointing unit normal. In addition, δ is a Dirac delta function, equal to unity at the interface and zero otherwise, and $\tilde{A}(\tilde{t})$ is the time-dependent interface area. The dimensionless groups that appear in the governing equations are defined as

$$Re=\frac{\rho U D_o}{\mu},\quad We=\frac{\rho U^2 D_o}{\sigma_s},\quad Fr=\frac{U^2}{gD_o},\quad Pe_s=\frac{U D_o}{D_s},\quad \beta_s=\frac{\mathcal{R}\mathcal{T}\Gamma_\infty}{\sigma_s},\quad h=\frac{H}{D_o}, \tag{5}$$

where Re, We, Fr, Pe_s and h stand for the Reynolds, Weber, Froude, (interfacial) Peclet numbers and the ratio between the liquid film thickness and the droplet diameter. Here, $\mathcal{R}$ is the ideal gas constant value ($\mathcal{R}=8.314$ J K^{-1} mol^{-1}), $\mathcal{T}$ denotes temperature, and D_s stands for the interfacial diffusion coefficient. Gravity is negligible during the impact as indicated by the Froude and the Bond number values, i.e. $Fr\sim\mathcal{O}(10^2)$, $Bo=\rho g D_0^2/\gamma<1$ (similar assumptions were made by Deegan et al. (2007)). The parameter β_s is the surfactant elasticity number that is a measure of the sensitivity of the surface tension, σ, to the interface surfactant concentration, Γ. The non-linear Langmuir equation is used to describe σ in terms of Γ (Manikantan and Squires, 2020), this is

$$\tilde{\sigma}=1+\beta_s\ln(1-\tilde{\Gamma}). \tag{6}$$

The Marangoni stress, $\tilde{\tau}$, is expressed as a function of $\tilde{\Gamma}$ as

$$\frac{1}{We}\nabla_s\tilde{\sigma}\cdot\mathbf{t}\equiv\frac{\tilde{\tau}}{We}=-\frac{Ma}{(1-\tilde{\Gamma})}\nabla_s\tilde{\Gamma}\cdot\mathbf{t}, \tag{7}$$

where $Ma=\beta_s/We=Re\mathcal{T}\Gamma_\infty/\rho U^2 D_o$ is the Marangoni parameter and $\mathbf{t}$ is the unit tangent to the interface.

Fig. 1b illustrates the domain and the initial conditions of the problem, which follows previous work by Josserand et al. (2016), Agbaglah and Deegan (2014), and Constante-Amores et al. (2023b). The droplet of diameter D_0 and velocity U impacts a uniform liquid layer of thickness H. The computational domain used in this study is $8D_0\times8D_0\times4D_0$, large enough to prevent artificial reflections at the boundaries. The droplet's centre is initially positioned slightly above the pool surface (e.g. $0.05D_0$ above the initial flat pool). A no-slip and no-penetration condition is applied to the bottom wall of the domain, while the top and lateral boundaries have a no-penetration condition, in line with the methodology of Batchvarov et al. (2021).

The numerical framework was previously validated against experimental data in Constante-Amores et al. (2023b), where it accurately reproduced the temporal evolution of the crown observed in the experiments of Che and Matar (2017). This validation covered a range of film thicknesses, Reynolds numbers, and Weber numbers. The framework has also been verified for drop-interface coalescence, representing the limiting case of drop impact onto a quiescent pool ($U=0$), as detailed in Constante-Amores et al. (2021). Furthermore, its capability to capture nonlinear interfacial dynamics has been demonstrated in studies of capillary breakup of liquid threads (Constante-Amores et al., 2020, 2021). Validation of the surfactant transport equations was reported in Shin et al. (2018). For the present simulations, we employ a grid resolution of $768^2\times384$, which has been shown to yield mesh-independent results (Constante-Amores et al., 2023b). Under this resolution, conservation errors for liquid volume and surfactant mass remain below 10^{-1}% and 10^{-2}%, respectively.

3. Results and discussion

In this section, we provide a detailed analysis of the impact dynamics of water-glycerol droplets on shallow pools containing various surfactants. Our findings are organised into three subsections. Section 3.1 presents the tensiometry measurements and an experimental regime map that details the different modes of crown evolution observed under various conditions, highlighting the interplay between the dynamic surface tension of the shallow pool and the impact parameters. Section 3.2 shows an experimental regime map of the crown evolution. Finally, Section 3.3 compares experimental results with 3D numerical simulations for the smooth surface to validate our approach and confirm the accuracy of our models. It also explores how the Peclet number influences crown evolution, using simulations to reveal the role of surfactant dynamics in droplet impact behaviour.

3.1. Tensiometry and empirical observations of crown evolution

Fig. 2 shows the dynamic surface tension measurements obtained using the MBP method for all the surfactant solutions in this study. Three distinct behaviours are observed for the Triton, SDS, and Surfynol solutions. For Triton, at times shorter than 10 ms, the dynamic surface tension is similar to that of the clean aqueous glycerol mixture, then it decreases monotonically, reaching a surface tension of approximately

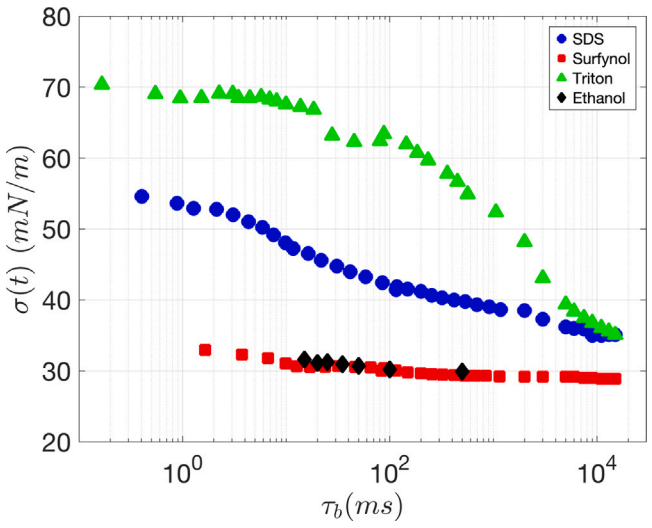

Fig. 2. Dynamic surface tension for the three surfactant solutions used in this work. The Triton solution until $\tau_b \approx 10$ ms, has approximately the same surface tension as the clean solution. However it has the same surface tension as the SDS solution at $\tau_b = 10$ s. The Surfynol solution has the lowest dynamic surface tension at all times, with $\sigma(t) \approx 33$ mN m^{-1} at $\tau_b = 1$ ms and $\sigma(t) \approx 29$ mN m^{-1} at $\tau_b = 10$ s. Ethanol 3.2 cP has a similar dynamic surface tension as the Surfynol solution.

35 mN m^{-1} at $\tau_b = 10$ s. The SDS solution shows a reduced surface tension of 55 mN m^{-1} compared to the aqueous glycerol mixture and continues to decrease until it matches the Triton solution's dynamic surface tension at $\tau_b = 10$ s. In contrast, Surfynol significantly reduces the surface tension of the aqueous glycerol solution to 33 mN m^{-1} at $\tau_b = 1$ ms and continues decreasing, reaching 28 mN m^{-1} at $\tau_b = 10$ s. The ethanol and glycerol solution, referred to as 'ethanol 3.2 cP' from here on, has a dynamic surface tension very similar to that of Surfynol, within the limits of our dynamics surface tension measurement. We classify SDS and Triton as *slow* surfactants because it takes at least 10 s for their solutions to reduce surface tension to roughly half that of a clean solution. In contrast, Surfynol is termed a *fast* surfactant, exhibiting rapid interfacial adsorption and a measurable decrease in surface tension on the order of 1 ms. As noted in the context of droplet-impact studies, the dynamic Leidenfrost behaviour of surfactant-laden drops is controlled by these same adsorption–desorption kinetics of surfactant molecules migrating from the bulk fluid to the interface and the resultant transient lowering of surface tension (Prasad et al., 2022).

In our experiments, we observed distinct qualitative differences in the behaviour of droplet impacts at the same velocity on a clean pool compared to surfactant-laden pools. Snapshots of experiments at $We = 256$ are presented in Fig. 3. For both the clean pool and the SDS 1 CMC pool, we observed crowns that do not break up into secondary droplets. However, the crown on the SDS 1 CMC pool exhibited more corrugation at the top compared to the clean pool (see Fig. 3b). In contrast, for the Triton 1 CMC pool, fingering was observed at $t = 5.5$ ms, which subsequently breakup into droplets at $t = 8.9$ ms. These differences between impacts on Triton and SDS pools arise even though both liquids have similar equilibrium surface tensions. However, at the crown-collapse timescales their dynamic surface tensions differ substantially ($\sigma(t_c) \approx 48$ mN m^{-1} for SDS and $\sigma(t_c) \approx 67$ mN m^{-1} for Triton). The different dynamics highlight the crucial role that dynamic surface tension plays at different stages post-impact. This leads to two key consequences: (i) During crown expansion new interface is created rapidly. The relatively slow adsorption kinetics of Triton (reflected in its dynamic surface tension behaviour) means that the freshly exposed surface is likely to remain starved of surfactant, while the bulk saturated regions retain high coverage. The resulting surface tension gradient is therefore greater for Triton than for SDS, driving stronger Marangoni flows along the crown rim that amplify finger formation and breakup. (ii) The surface elasticity $E = -\frac{\partial \sigma}{\partial \ln \Gamma}$ quantifies how sensitively σ responds to local concentration changes. Because $\sigma(t_c)$ is almost double the equilibrium surface tension for Triton, localised *rigidification* resist uniform retraction, promoting non-uniform thinning and more pronounced corrugations. In contrast, SDS adsorbs more rapidly than Triton during the first 10 ms, partially replenishing newly created interface and smoothing the surface tension gradients, leading to milder Marangoni stresses and a smoother crown than for the Triton solution for the same Weber number.

The impact on the Surfynol 1 CMC pool, showed even more pronounced differences compared to the clean case: secondary droplets appeared as early as $t = 2.2$ ms, with the formation of fingers that grow ($t = 5.5$ ms) and subsequently breakup ($t = 8.9$ ms) (see Fig. 3c). One might attribute the observed phenomena with Surfynol to the reduction in surface tension. To investigate this further, we conducted additional experiments using ethanol and glycerol (see Fig. 3d). The impact dynamics result in the regime of a separate ejecta sheet (Sykes et al., 2023) and the crown breaks up before forming fingers and collapsing. As ethanol 3.2 cP and the Surfynol solution have nearly the same surface tension but exhibit completely different behaviours, then surface tension lowering alone cannot possibly be responsible for the difference in outcome across the solutions. Instead, the Marangoni stresses that arise from surface tension gradients due to surfactant concentration gradients, may play a crucial role in the dynamics of surfactant-laden systems.

3.2. Experimental interfacial regime map

We now present our analysis to map out the full range of crown behaviours – splashing, recoiling breakup and non-breaking – across impact velocities and surfactant types. Here, a *clean* drop of an aqueous solutions of glycerol (μ=3.2 cP) impacts a pool of the same liquid in which, for each set of experiments, a surfactant (one of the three used in this study, as described in the Methods section) was added. Upon varying the impact velocity, we identified three distinct types of crown formation and evolution after impact: splashing, recoiling breakup, and non-breaking or smooth crown. 'Splashing' refers to the scenario where the crown forms and secondary droplets are ejected from its top as it expands. 'Recoiling breakup' occurs when fingers form on the crown, and during the crown's retraction, these fingers break into droplets. The 'smooth crown' regime describes a crown that remains intact during both formation and recoil; although fingers may form, they do not break up.

We present a regime map illustrating the outcome of the impact based on the Weber number and the type of surfactant added to the shallow pool (see Fig. 4). The regime map displays the Weber number We_D in terms of the pool dynamic surface tension at the typical time of crown collapse $t_c \approx 10$ ms, $\sigma(t_c)$. In this way, the leftmost points represent the Surfynol solution, followed by the ethanol, SDS and Triton solutions, while the rightmost points correspond to the clean case.

For the Surfynol pool ($\sigma(t_c) = 31$ mN m^{-1}), the transition between non-breaking and recoiling breakup, as well as splashing, occurs at the lowest Weber numbers of all the surfactant laden liquid pools. Specifically, these transitions are observed at $We = 209$ and $We = 256$, respectively. Ethanol, as a pure liquid, splashes at the lowest We_D with no recoiling breakup, underscoring how low equilibrium surface tension alone can drive immediate splashing and highlighting that, for surfactant-laden systems like Surfynol, sub-millisecond adsorption kinetics may modulate the very early dynamics (< 1 ms) of crown formation.

For the SDS and Triton pools, with surface tensions of $\sigma(t_c) = 48$ mN m^{-1} and $\sigma(t_c) = 67$ mN m^{-1} respectively, the transitions occur at similar Weber numbers despite the differences in surface tension at $\tau_b = 10$ ms. The similarities can be explained by the similar surface tension that both of the surfactants have at $\tau_b = 10$ s, $\sigma(10\text{ s}) \approx 35$

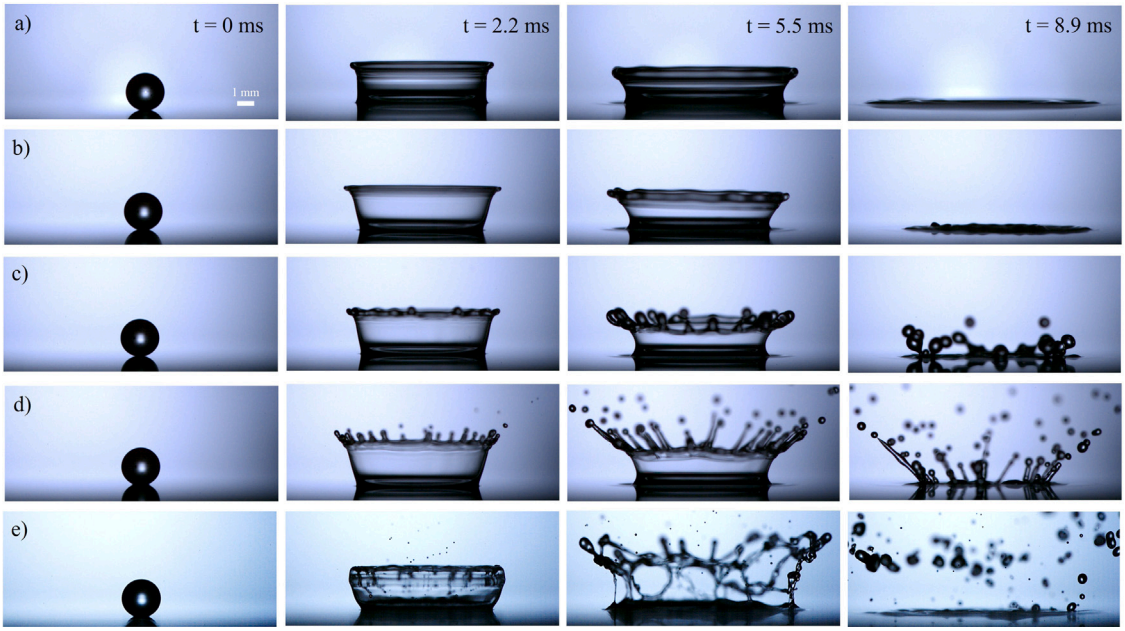

Fig. 3. Impact dynamics on the "clean", the surfactant laden and the ethanol glycerol mix pools at $We = 256$ and $Re = 2314$. (a) "Clean" aqueous glycerol, (b) SDS at 1 CMC, (c) Triton at 1 CMC, (d) Surfynol at 1 CMC and e) ethanol and glycerol. The clean aqueous glycerol mix and the SDS, present a smooth crown. In contrast, for Triton we observe recoiling breakup, due to uneven distribution of the surfactant in the rim (Constante-Amores et al., 2023a). For Surfynol, we observe splashing and recoiling breakup. The ethanol and glycerol pool displays a separate ejecta sheet and the crown breaks up before forming fingers.

mN m^{-1} . Since, the droplet impacts at an already equilibrated surface, the transition between splashing and no splashing is expected to be governed by the equilibrium surface tension, or a value close to it. As the SDS and Triton pools, can be classified as slow surfactants, the splashing transition correlates primarily with their common equilibrium surface tension ($\sigma_{eq} \approx 35$ mN m^{-1}), rather than the differing $\sigma(t_c)$, because their adsorption kinetics are too slow to significantly replenish the rapidly expanding interface during the time of crown formation. Although the transitions, occur at similar Weber numbers, we note that the morphology of the impact can differ slightly as observed in Fig. 3. The difference in morphology arises from a difference in the changes of surface tension and Marangoni flows generated due to the difference in dynamic surface tension curves. For the surfactant-free pool ($\sigma(t_c) = 69$ mN m^{-1}) exhibits the highest Weber numbers for transitions between non-breaking and recoiling breakup, as well as recoiling breakup and splashing. Additionally, we observe instances where both smooth and recoiling breakup can occur. Near the critical Weber number delineating smooth recoil and recoiling breakup, small experimental fluctuations in impact speed or local surfactant coverage lead to a mixed occurrence of both behaviours. Statistical analysis over multiple repeats confirms that the observed overlap represents a narrow transitional regime.

These observations align with previous findings that surfactants can significantly alter the splashing characteristics of droplets (Varghese et al., 2024). This effect is particularly pronounced for Surfynol, which reduces the surface tension of the aqueous glycerol mixture the most, cutting it by more than half at $\tau_b = 1$ ms. In contrast, when polymeric droplets – such as polyacrylamide solutions – impact either polymeric or water films, viscoelastic effects (likely due to high shear stresses encountered during impact) inhibit ligament formation and breakup, effectively suppressing splashing (Singh et al., 2025; Mohammad Karim, 2020). These results emphasise the critical role of surfactants in affecting the dynamics of droplet impacts and the crown evolution, providing valuable insights for controlling splash behaviour in applications like 3D printing and coatings.

3.3. 'Smooth' regime: numerical simulations with SDS surfactant

To get more insight on the surfactant effect we compare the experiments and the numerical simulations for a surfactant-free pool, and when the pool is loaded with SDS, for the case in which the crown does not break as in Fig. 3 (a) and (b). We note that in the experiments we used soluble surfactants. However, SDS can be considered effectively insoluble for droplet impact phenomena. This is because the solubility of SDS has minimal impact on the surface concentration and its gradients along the interface. The timescale for SDS adsorption from the bulk to the surface is approximately 100 ms, whereas the timescales for impact, Marangoni effects, and flow dynamics – whether inertial-capillary, inertial-viscous, or viscous – are all on the order of just a few milliseconds (Kamat et al., 2018). For a water-droplet of a typical size of $D_0 \sim \mathcal{O}(10^{-3})$m, the impact time scale $T_{imp} = t_r = D_0/U \sim \mathcal{O}(10^{-4} - 10^{-3})$s; whereas the Marangoni time-scale T_τ can be estimated by a balance between the Marangoni and the viscous stresses, resulting in $T_\tau \sim \mu D^2/(h\Delta\sigma) \sim \mathcal{O}(10^{-4} - 10^{-3})$s. As a result, the slower adsorption process does not play a significant role, supporting the assumption that SDS behaves as an insoluble surfactant in this context. Numerical simulations with other surfactants, such as Surfynol and Triton, are not included because they cannot be considered insoluble. Triton, for example, shows a much steeper decrease in dynamic surface tension over time compared to the smoother behaviour of SDS. Surfynol, on the other hand, diffuses very rapidly to the interface and causes a sharp drop in surface tension, leading to strong gradients and pronounced Marangoni stresses. The primary reason for not performing numerical simulations with soluble surfactants is the difficulty in obtaining accurate experimental parameters, such as bulk diffusivity and adsorption–desorption rates, which are essential for achieving a good match in the simulations.

Fig. 5a presents snapshots of the interface location for a surfactant-free case characterised by $We = 244$, $Re = 1861$, and $h = 0.11$. We observe that at the early stages of the dynamics, a vertical ejecta sheet is formed due to the large inertia from the droplet impacting the motionless liquid pool (see first panel of Fig. 5a). The capillary

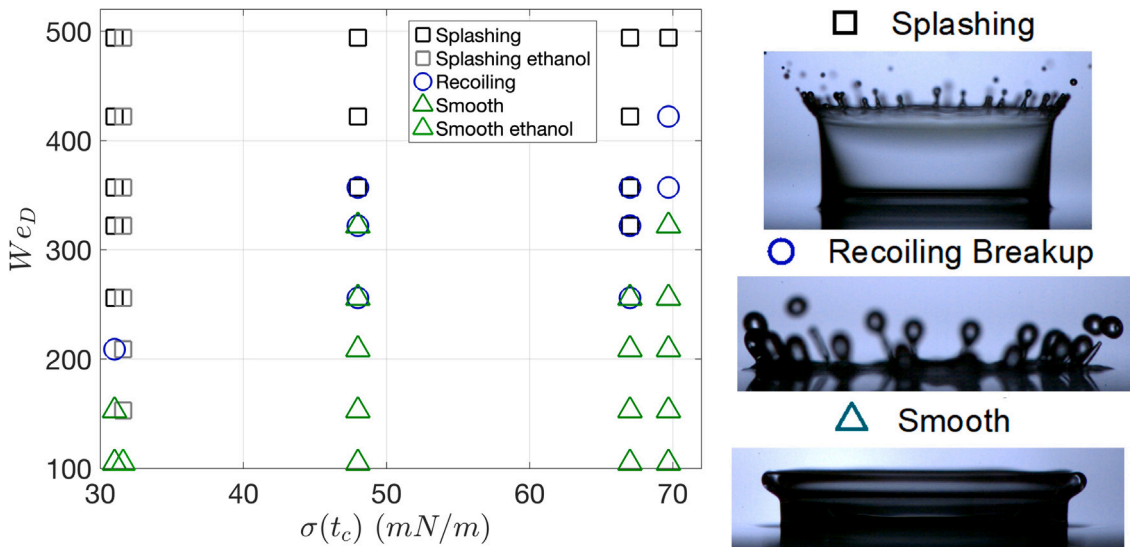

Fig. 4. Regime map exploring the crown formation and outcomes in terms of the dynamic surface tension taken at the characteristic time for crown collapse t_c, and the Weber based on the droplet characteristics. From left to right, the data series correspond to Surfynol, surfactant-free 3.2 cP ethanol, SDS, Triton, and the surfactant-free glycerol baseline. Both SDS and Triton exhibit a lower transition point to splashing and receding breakup compared to water. However, we observe qualitative differences in the crown's smoothness due to variations in dynamic surface tension. Among all the liquids studied, Surfynol has the lowest Weber number for the transition to splashing—approximately half that of water. This is because Surfynol significantly reduces surface tension to its lowest value ($\approx$ 30 mN m^{-1}) and acts rapidly, lowering the surface tension of the impacting droplet within the first milliseconds of impact. This rapid reduction in surface tension makes the interface more prone to fragmentation. Ethanol, splashes at the lowest We_D with no recoiling breakup.

retraction in the tip of the ejecta sheet gives rise to the formation of a rim where the liquid accumulates (see second panel of Fig. 5a).

The rim destabilises due to a Rayleigh-Plateau instability, leading to the development of corrugations along its edge (see the third panel of Fig. 5a). In this particular case, the corrugations do not detach to form ligaments, likely because the timescale for ligament formation is much longer than the retraction timescale of the ejecta sheet. The retraction of the ejecta sheet ultimately results in the rim's coalescence with the pool (see the four panels of Fig. 5a). In the bottom panels of Fig. 5a, we have also included the numerical predictions, which accurately capture the complex dynamics observed in the experiment. This includes the formation of the ejecta sheet, the development and destabilisation of the rim, and the eventual coalescence of the rim with the pool.

Next, we move to the surfactant-driven effects due to the presence of SDS in the pool. We have considered insoluble surfactants whose critical micelle concentration (CMC) is $\Gamma_\infty \sim \mathcal{O}(10^{-5})$ mol m^{-2} (see Chang and Franses (1995)). Then, the surfactant strength parameter β_s at room temperature is $\beta_s \approx 0.4$. In the simulations, we define the initial (dimensionless) surfactant concentration Γ_0 depending on Γ_∞, and it is expressed as $\Gamma = \Gamma_0/\Gamma_\infty$. In the experiments, even though the total amount of surfactant exceeds the CMC, the monomer concentration stays at the level corresponding to the CMC, as the additional surfactant molecules form micelles (Berg, 2009). The initial surface concentration of SDS, is defined as the surface concentration at equilibrium with a bulk concentration at 1 CMC (as given by the experiments). This value is directly obtainable from surface tension measurements. According to Roché et al. (2009), the surface tension for an SDS solution at a bulk concentration of 2 CMC is $\tilde{\sigma}_0 = 40$, mN m^{-1} . Thus, the dimensionless initial surface tension is given by $\sigma_0 = \tilde{\sigma}_0/\sigma_s = 0.67$. This allows for the determination of the initial dimensionless surface concentration using the equation of state, Eq. (6), given a value of $\Gamma_0 \approx 0.56$. Finally, typical values of surface Peclet number Pe_s for aqueous surfactant systems lie in the range 10–10^6, as described in Liao et al. (2006). In this work we will take conservative values for the simulations: $\Gamma_0/\Gamma_\infty = 0.5$, $Pe_s = 10 - 1000$ and $\beta_s = 0.5$.

Fig. 5 (b) shows the temporal evolution of the surfactant-laden case with the parameters described earlier. Similar to the surfactant-free case, we observe the formation of the ejecta sheet, the development of the rim, its destabilisation into corrugations, and the eventual recoiling with the pool. However, the presence of surfactant causes the interface to become more rigid, leading to a delay in the dynamics. Another key difference is that the surfactant induces the formation of more corrugations in the rim. This increase in the number of corrugations is due to the uneven distribution of surfactant, which creates gradients in surface tension. These gradients result in diverging and converging motions caused by Marangoni stresses as they attempt to equalise the surfactant distribution at the interface. Similar phenomena were observed in Constante-Amores et al. (2023b). Turning our consideration to the numerical simulations, we observe that the simulations can capture the delay of the dynamics and the formation of more corrugations in the rim as observed in the experiments.

Finally, Fig. 5c shows the temporal evolution of the crown by tracking its vertical position $z(t)$ over time, comparing numerical simulations with experimental measurements for both clean and SDS-laden interfaces. In the absence of surfactants, the clean case exhibits a slightly lower trajectory than the surfactant-laden case. The presence of SDS leads to a noticeable increase in the interface height and a slower decay, consistent with the expected influence of surfactant-laden Marangoni stresses. The reason of the higher height comes from the uniform surfactant distribution along the interface (and shown in the following paragraphs). Fig. 6 shows that a higher Γ at the base of the sheet compared to the pool. This uneven Γ distribution leads to the generation of Marangoni stresses that act from the pool towards the crown. These stresses drive fluid along the interface into the sheet, effectively injecting momentum and mass into the sheet. As a result, Marangoni stresses promote lateral spreading of the sheet and help sustain its elevated height during the later stages of the dynamics. In both cases, the simulations closely match the experimental data, demonstrating that the numerical model accurately captures the interfacial dynamics and the influence of surfactants in this regime.

Having established that the numerical simulations, both with and without SDS surfactant, closely reproduce the experimental results in the smooth regime, we now leverage the simulations to isolate the role

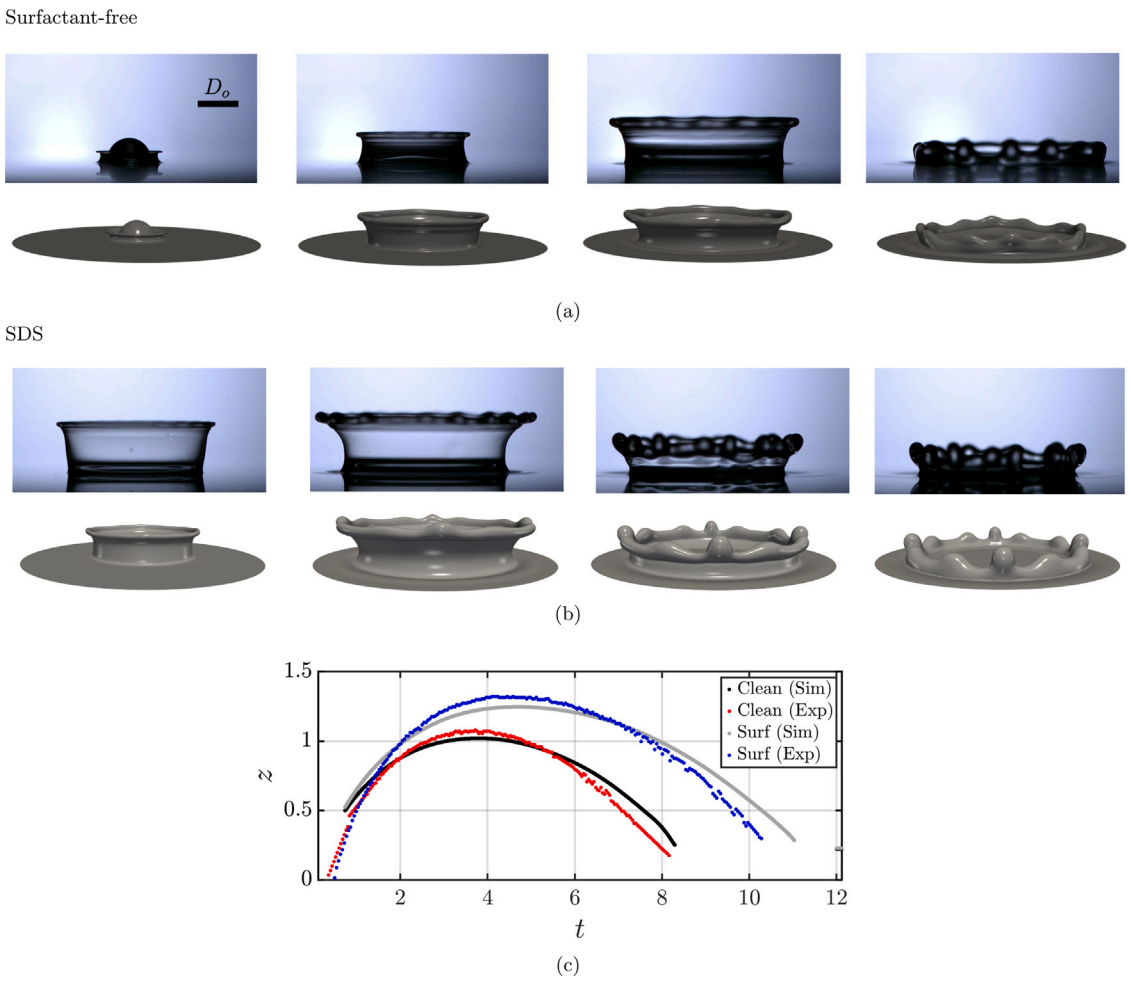

Fig. 5. Droplet impact with $Re = 1861$, $We = 244$, and $h = 0.11$. The spatiotemporal evolution of the interface location is shown for the surfactant-free case (panel a) and the surfactant-laden case with SDS (panel b). The top panels display the experimental snapshots, while the bottom panels present the numerical predictions. Panel c shows the temporal evolution of the vertical position of the crown. Here, D_0 corresponds to 2.2 mm, which is the scale shown in panel (a).

of surfactant transport kinetics. In particular, we systematically vary the surface Péclet number, Pe_s.

The focus on the Peclet number is driven by our aim to examine the relative importance of advective versus diffusive transport of surfactants at the interface. At lower Peclet numbers, diffusion dominates, leading to a more uniform distribution of surfactants and minimising the resulting Marangoni stresses. While, at higher Peclet numbers, advection becomes the primary transport mechanism, potentially creating sharp surfactant gradients and subsequently stronger Marangoni stresses at the interface— precisely the mechanism we infer from the enhanced rim corrugation seen in our SDS experiments. By comparing these simulations directly to the clean-pool case, we can quantify how transport kinetics alone delay the ejecta-sheet evolution, alter corrugation patterns, and modify recoil dynamics. We can also relate the Peclet number to the dynamic surface tension. After the impact, a significant amount of surface area is generated in a short period. This newly created surface is initially (nearly) free of surfactant, depending on the rate in which surfactant spreads, there will be different dynamics for either 'fast' or 'slow' surfactants.

Fig. 6 represents the effect of the surfactants through the analysis of the Pe_s with $Re = 1861$, $We = 244$, $h = 0.11$, $\beta_s = 0.5$ and $\Gamma_0 = \Gamma_\infty/2$ up to $t = 7.5$. It is also worth mentioning that all surfactant simulations have been carried out until the recoiling of the rim with the pool is observed. We observe that the dynamics of the surfactant-laden cases follow closely those of the surfactant-free case, with the formation of the ejecta sheet, the rim and its destabilisation to form corrugations to eventually the recoiling of the rim with the pool. As soon as the droplet impacts the pool, we observe the higher surfactant concentration in the apex of the droplet and the outer walls of the ejecta sheet. By increasing Pe_s, surfactant gradients along the interface are enhanced as displayed in Fig. 6, for $Pe_s = 100$ and $Pe_s = 1000$, respectively, in comparison to $Pe_s = 10$ where gradients in concentration are reduced. At later times, surfactant predominantly accumulates in the rim. A clear effect of varying Pe_s is that surfactant concentration gradients, and the associated transport, appear to suppress the number of corrugations observed in the rim. In the following sections, we will analyse and quantify the effects of Marangoni stresses.

The next part of the analysis focuses on the time evolution of a two-dimensional projection of the interfacial shape, Γ, the Marangoni stresses τ, and the tangential component of the interfacial velocity, u_{tz}, at $t = 1$, as presented in Fig. 7. First, we focus on early times to highlight the initial distribution of surfactant and the role of Pe_s. The first observation is that surfactants delay the dynamics, as seen in the two-dimensional projection of the interfacial shape. This delay mirrors the experimental snapshots at $t = 2.2$ ms, where the clean pool crown is already expanding smoothly (Fig. 3a), whereas the SDS-laden crown is just beginning to rise and already shows small corrugations (Fig. 3b).

It appears that Pe_s does not play a major role in determining the interface location, but all surfactant-laden cases differ from the surfactant-free case. The primary effect of surfactants can be observed in the accumulation at the droplet's apex. Higher values of Pe_s correspond to steeper gradients in Γ (see panel c), leading to a localised

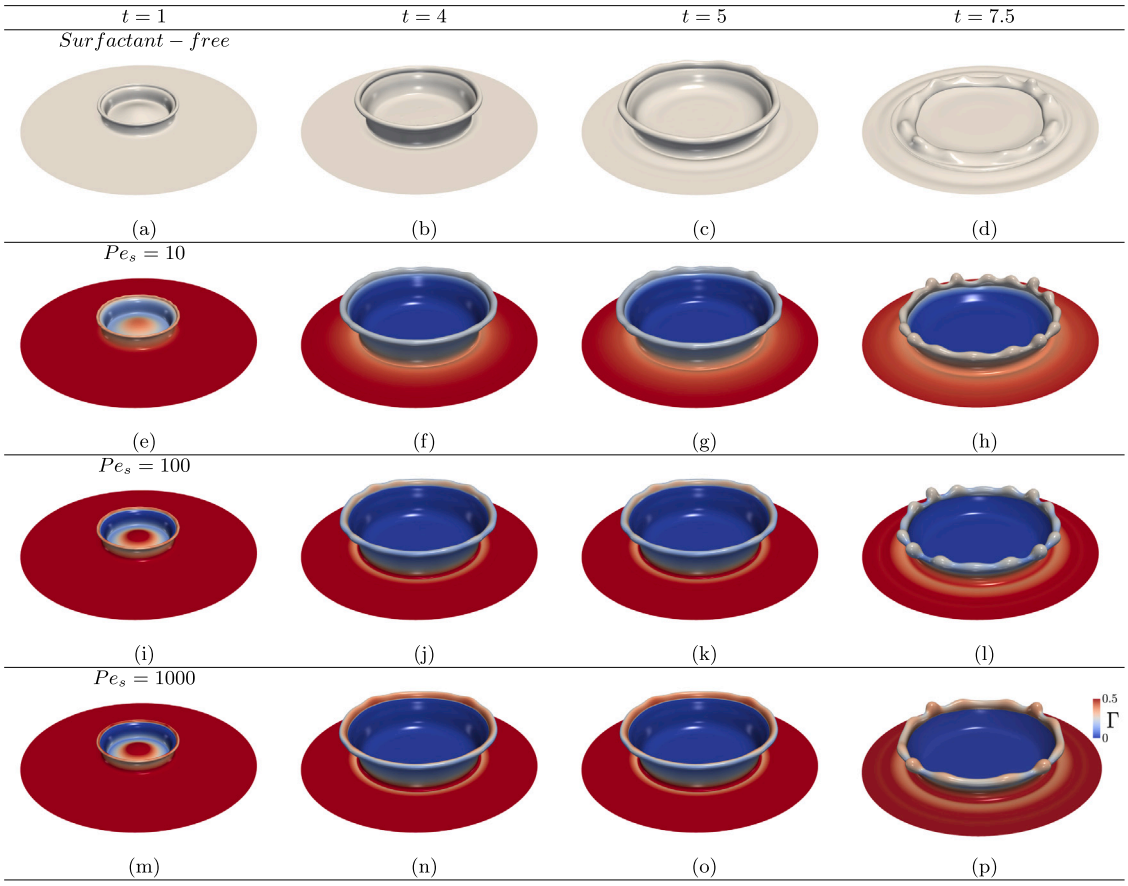

Fig. 6. Effect of Pe_s on the drop impact dynamics for insoluble surfactants. Spatio-temporal evolution of the three-dimensional interface shape for surfactant-free cases, (a)–(d), and surfactant-laden cases for $Pe_s = (10, 100, 1000)$ corresponding to panels (e)–(h), (i)–(l) and (m)–(p), respectively. Here, the dimensionless parameters are $Re = 1861$, $We = 244$ and $h = 0.11$. For the surfactant-laden cases, $\beta_s = 0.5$ and $\Gamma_0 = \Gamma_\infty/2$, the colour indicates the value of Γ, and the legend is shown in panel (p).

decrease in τ. These local gradients in Γ result in a pronounced peak in the τ profile at the droplet's apex and near the rim, with the peak being most significant for the highest Pe_s value of 1000, as shown in Fig. 7d.

Next, we focus on later times when capillary forces dominate the dynamics of the phenomena. Fig. 8 shows the two-dimensional projection of the interfacial shape, Γ_s, the Marangoni stresses τ, and the tangential component of the interfacial velocity, u_{tz}, at $t = 5$. We observe similar behaviour as at $t = 1$. The surfactant-induced effects cause retardation of the dynamics, resulting in a taller jet sheet (see panel 8a). As the Peclet number increases, steeper gradients develop in the surfactant profiles (see panel 8c), leading to larger Marangoni stresses (see panel 8d) and greater tangential velocity due to the uneven surfactant distribution (see panel 8b). These enhanced flows further destabilise the rim, producing the multiple corrugations that remain below the breakup threshold in both simulation and experiment.

Finally, we explore the temporal changes in the total interfacial area and the kinetic energy $E_k = \rho \int_V \mathbf{u}^2/2dV$ normalised by their initial values, as shown in Fig. 9. Initially, there is a linear change in the interfacial area as time evolves, with similar behaviour for both clean and surfactant-laden cases up to $t \lesssim 2$. However, beyond this point, the evolution of the interfacial area is significantly affected by the presence of surfactants. By inspecting their trend, we can conclude that the addition of surfactants leads to a larger area generation due to the rigidifying effect brought via Marangoni stresses. This maximum area corresponds to the largest vertical stretch of the crown before it starts recoiling.

A monotonic increase of surface area with Pe_s, highlighting the enhanced deformation induced by surfactant effects. Notably, the peak interfacial area in surfactant-laden cases exceeds that of the surfactant-free case by approximately 5%. The temporal evolution of the kinetic energy mirrors that of the interfacial area, exhibiting a minimum when the interfacial area attains its maximum—consistent with the conversion of kinetic energy into interfacial energy, and vice versa during subsequent relaxation.

4. Conclusions

Using a combination of experiments and numerical simulations, we have shown that surfactants have a significant effect on the morphology and evolution of the archetypal crown that develops following the impact of a surfactant-free droplet onto a surfactant-laden pool. With three different surfactants (SDS, Triton X-100, and Surfynol 465), we varied the dynamic surface tension of the pool on the time scale of crown collapse t_c, from 30 to 69 mN m^{-1}. A $We - \sigma$ regime map (Fig. 4) reveals three distinct post-impact regimes: 'smooth' receding of the sheet, 'recoiling' breakup, and 'splashing'. Most notably, impacts on Surfynol-laden pools (our fastest surfactant) resulted in splashing and recoiling breakup at the lowest Weber numbers, compared to other (slower) surfactants and the surfactant-free control (an aqueous glycerol mix). By using a surfactant-free 3.2 cP ethanol with the same surface tension at t_c as the Surfynol solution, we observe distinct splash behaviours: the ethanol crown disintegrates, whereas the Surfynol solution produces fingering and recoiling breakup. This observation demonstrates that rapidly adsorbing surfactants can alter post-impact dynamics compared to a clean base fluid.

Our numerical simulations – carefully validated against our experiments in the cases of most interest (Fig. 5) – of the smooth receding

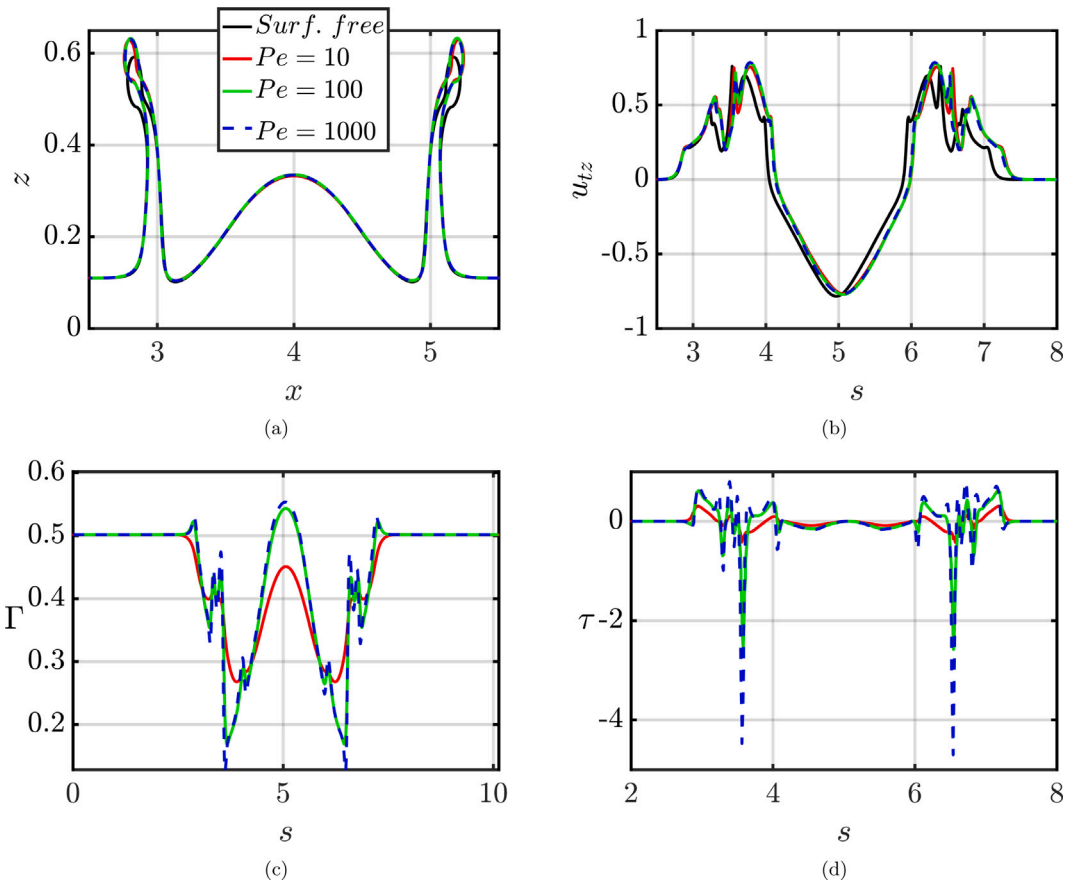

Fig. 7. Effect of Pe_s on the flow dynamics at $t = 1$. Two-dimensional projections of the interface, u_{tz}, Γ and τ in the $x--z$ plane ($y = 4$) are shown in $(a)-(d)$, respectively. Note that the abscissa in (a) corresponds to the x coordinate, and in $(b)-(d)$ to the arc length, s. The arc length s corresponds to the x–z plane ($y = 4$) intersecting the interface. All parameters remain unchanged from Fig. 6.

regime, both in the surfactant free and surfactant-laden (for SDS, which can be considered insoluble) cases, confirmed that surfactants slow down the dynamics of crown formation and collapse. As the Peclet number increases, Marangoni stresses become more significant, leading to a taller and narrower crown compared to the surfactant-free case. The effect of the surfactant itself was confirmed by analysing the evolution of the interfacial area and kinetic energy, showing that the presence of surfactants results in approximately 5% greater interfacial area generation and a corresponding decrease in kinetic energy compared to the clean case, with the surface area increasing monotonically with Pe.

By integrating high-speed experiments with 3D numerical simulations, we have shown that surfactant driven changes in interfacial tension - dynamic at the moment of crown collapse t_c for fast-adsorbing surfactants and equilibrium for slow-adsorbing ones — reliably predict whether a crown will splash. In the case of slow-adsorbing surfactants, their slow adsorption kinetics preclude significant tension reduction during crown formation, so the splashing threshold instead corresponds to their equilibrium surface tension. Our results reveal that surfactants alter the rim instability, shifting the breakup mode from crown fragmentation to fingering and recoil. Moreover, we have connected these observations to surfactant transport through the Peclet number, demonstrating how diffusion and advection balance to control surface coverage during the critical early stages of impact. Such droplet dynamics play a crucial role in both natural and industrial applications, as the resulting fluid fragmentation leads to the formation of smaller droplets that carry mass, momentum, and energy, facilitating fluid transfer from the pool to the surrounding atmosphere. Therefore, our findings provide valuable insights into splash dynamics, with potential applications in optimising processes such as 3D printing, coatings, and inkjet printing, where controlling droplet behaviour is crucial for achieving precision and efficiency.

CRediT authorship contribution statement

Miguel A. Quetzeri-Santiago: Writing – original draft, Visualization, Validation, Project administration, Methodology, Investigation, Formal analysis, Data curation, Conceptualization. **C. Ricardo Constante-Amores:** Writing – original draft, Software, Methodology, Investigation, Formal analysis, Data curation, Conceptualization. **Thomas C. Sykes:** Writing – review & editing, Methodology, Investigation, Conceptualization. **Seungwon Shin:** Writing – review & editing, Software, Resources, Methodology. **Jalel Chergui:** Writing – review & editing, Software, Resources, Methodology. **Damir Juric:** Writing – review & editing, Software, Resources, Methodology. **J. Rafael Castrejón-Pita:** Writing – review & editing, Resources, Project administration, Funding acquisition, Conceptualization. **Alfonso A. Castrejón-Pita:** Writing – review & editing, Supervision, Resources, Project administration, Methodology, Funding acquisition, Conceptualization.

Declaration of competing interest

The authors declare that they have no known competing financial interests or personal relationships that could have appeared to influence the work reported in this paper.

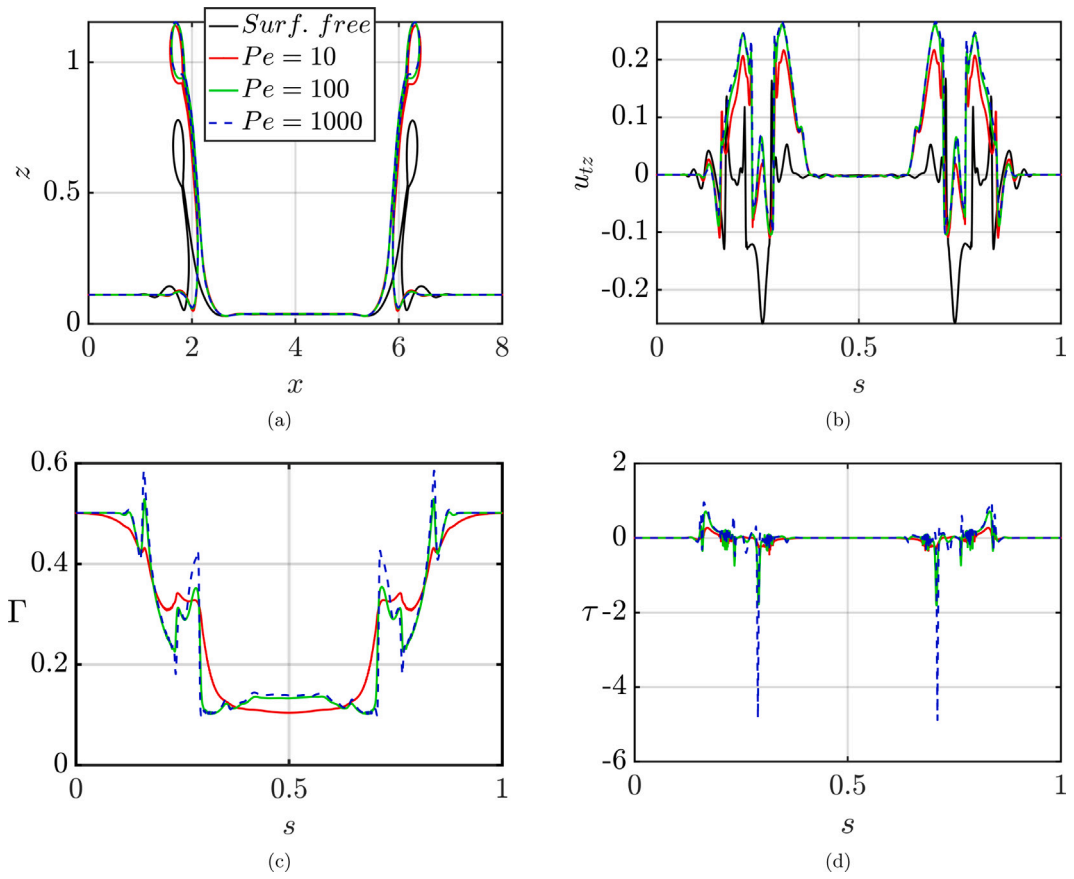

Fig. 8. Effect of Pe_s on the flow dynamics at $t = 5$. Two-dimensional projections of the interface, u_{tz}, Γ and τ in the $x--z$ plane ($y = 4$) are shown in $(a)-(d)$, respectively. Note that the abscissa in (a) corresponds to the x coordinate, and in $(b)-(d)$ to the arc length, s. The arc length s corresponds to the x–z plane ($y = 4$) intersecting the interface, s has been normalised on the full extent of s associated with the length of the impact region in each case. All parameters remain unchanged from Fig. 6.

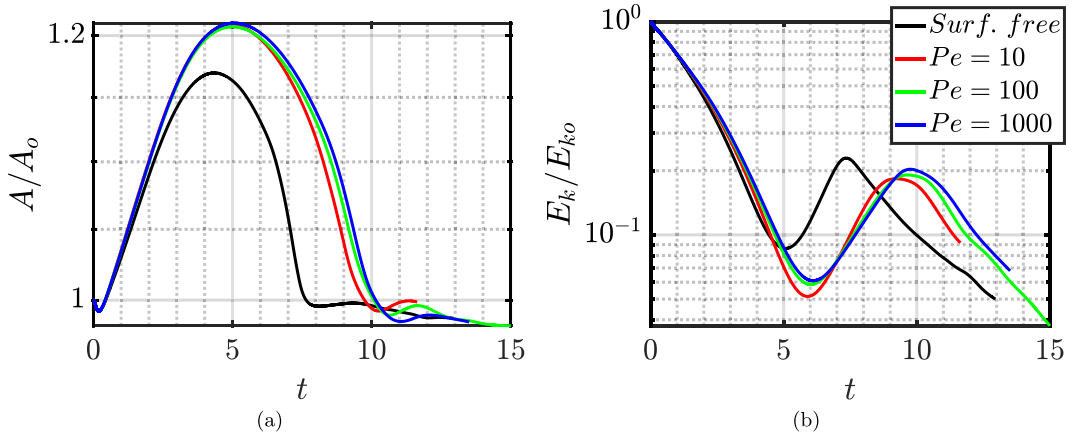

Fig. 9. Temporal evolution of the total interfacial area, (a), and the kinetic energy, (b), normalised by their initial values, for the surfactant-free and surfactant-laden cases. All parameters remain unchanged from Fig. 6.

Acknowledgements

M.A.Q-S. acknowledges support from DGAPA through Subprograma de Incorporación de Jóvenes Académicos de Carrera (SIJA) and through the grant PAPIIT-UNAM IA101025. D.J. and J.C. acknowledge support through HPC/AI computing time at the Institut du Developpement et des Ressources en Informatique Scientifique (IDRIS) of the Centre National de la Recherche Scientifique (CNRS), France, coordinated by GENCI (Grand Equipement National de Calcul Intensif) grant 2025 A0182B06721. T.C.S. and A.A.C-P. acknowledge funding from the NSF/CBET-EPSRC (Grant Nos. EP/W016036/1 and EP/S029966/1). During the preparation of this work the authors used ChatGPT in order to improve the text readability. After using this tool/service, the authors reviewed and edited the content as needed and take full responsibility for the content of the publication.

Data availability

Data will be made available on request.

References

Agbaglah, G., Deegan, R., 2014. Growth and instability of the liquid rim in the crown splash regime. J. Fluid Mech. 752, 485–496.

Ananthakrishnan, P., Yeung, R.W., 1994. Nonlinear interaction of a vortex pair with clean and surfactant-covered free surfaces. Wave Motion 19 (4), 343–365.

Batchvarov, A., Kahouadji, L., Constante-Amores, C.R., Norões Gonçalves, G.F., Shin, S., Chergui, J., Juric, D., Craster, R.V., Matar, O.K., 2021. Three-dimensional dynamics of falling films in the presence of insoluble surfactants. J. Fluid Mech. 906 (A16).

Berg, J.C., 2009. An Introduction To Interfaces and Colloids. WORLD SCIENTIFIC.

Bergeron, V., Bonn, D., Martin, J.Y., Vovelle, L., 2000. Controlling droplet deposition with polymer additives. Nature 405 (6788), 772–775.

Blanchard, D.C., Syzdek, L.D., 1972. Concentration of bacteria in jet drops from bursting bubbles. J. Geophys. Res. 77 (27), 5087–5099.

Chang, C., Franses, E., 1995. Adsorption dynamics of surfactants at the air/water interface: a critical review of mathematical models, data, and mechanisms. Colloids Surfaces A: Physicochem. Eng. Asp. 100, 1–45.

Che, Z., Matar, O.K., 2017. Impact of droplets on liquid films in the presence of surfactant. Langmuir 33 (43), 12140–12148.

Cheng, X., Sun, T.-P., Gordillo, L., 2022. Drop impact dynamics: Impact force and stress distributions. Annu. Rev. Fluid Mech. 54 (1), 57–81.

Constante-Amores, C.R., Chergui, J., Shin, S., Juric, D., Castrejón-Pita, J., Castrejón-Pita, A.A., 2022. Role of surfactant-induced marangoni stresses in retracting liquid sheets. J. Fluid Mech. 949 (A32).

Constante-Amores, C.R., Kahouadji, L., Batchvarov, A., S, S., Chergui, J., Juric, D., Matar, O.K., 2020. Dynamics of retracting surfactant-laden ligaments at intermediate ohnesorge number. Phys. Rev. Fluids 5, 084007.

Constante-Amores, C., Kahouadji, L., Batchvarov, A., Shin, S., Chergui, J., Juric, D., Matar, O., 2021. Direct numerical simulations of transient turbulent jets: vortex-interface interactions. J. Fluid Mech. 922 (A6).

Constante-Amores, C., Kahouadji, L., Shin, S., Chergui, J., Juric, D., Castrejón-Pita, J., Matar, O., Castrejón-Pita, A., 2023a. Impact of droplets onto surfactant-laden thin liquid films. J. Fluid Mech. 961 (A8).

Constante-Amores, C., Kahouadji, L., Shin, S., Chergui, J., Juric, D., Castrejón-Pita, J., Matar, O., Castrejón-Pita, A., 2023b. Impact of droplets onto surfactant-laden thin liquid films. J. Fluid Mech. 961 (A8).

Cossali, G.E., Coghe, A., Marengo, M., 1997. The impact of a single drop on a wetted solid surface. Exp. Fluids 22 (6), 463–472.

Craster, R., Matar, O., Papageorgiou, D., 2002. Pinchoff and satellite formation in surfactant covered viscous threads. Phys. Fluids 14 (4), 1364–1376.

Deegan, R.D., Brunet, P., Eggers, J., 2007. Complexities of splashing. Nonlinearity 21 (1), C1–C11.

Deike, L., Ghabache, E., Liger-Belair, G., Das, A.K., Zaleski, S., Popinet, S., Séon, T., 2018. Dynamics of jets produced by bursting bubbles. Phys. Rev. Fluids 3 (1), 013603.

Edgerton, H., 1977. Stopping Time: The Photographs of Harold Edgerton Abrams. New York.

Ersoy, N.E., Eslamian, M., 2020. Phenomenological study and comparison of droplet impact dynamics on a dry surface, thin liquid film, liquid film and shallow pool. Exp. Therm. Fluid Sci. 112, 109977.

Fainerman, V.B., Miller, R., 1998. The maximum bubble pressure tensiometry. In: Studies in Interface Science, vol. 6, Elsevier, pp. 279–326.

Fudge, B.D., Cimpeanu, R., Castrejón-Pita, A.A., 2021. Dipping into a new pool: The interface dynamics of drops impacting onto a different liquid. Phys. Rev. E 104 (6), 065102.

Gilet, T., Bourouiba, L., 2015. Fluid fragmentation shapes rain-induced foliar disease transmission. J. R. Soc. Interface 12 (104), 20141092.

Herczyński, A., Cernuschi, C., Mahadevan, L., 2011. Painting with drops, jets, and sheets. Phys. Today 64 (6), 31–36.

Hoffman, H., Sijs, R., de Goede, T., Bonn, D., 2021a. Controlling droplet deposition with surfactants. Phys. Rev. Fluids 6 (3), 033601.

Hoffman, H., Sijs, R., de Goede, T, Bonn, D., 2021b. Controlling droplet deposition with surfactants. Phys. Rev. Fluids 6, 033601.

Jiang, X., Rotily, L., Villermaux, E., Wang, X., 2022. Submicron drops from flapping bursting bubbles. Proc. Natl. Acad. Sci. 119 (1), e2112924119.

Josserand, C., Ray, P., Zaleski, S., 2016. Droplet impact on a thin liquid film: anatomy of the splash. J. Fluid Mech. 802, 775–805.

Kamat, P.M., Wagoner, B.W., Thete, S.S., Basaran, O.A., 2018. Role of marangoni stress during breakup of surfactant-covered liquid threads: reduced rates of thinning and microthread cascades. Phys. Rev. Fluids 3 (4), 043602.

Kroeze, T.B., Rivas, D.F., Quetzeri-Santiago, M.A., 2024. Microfluidic jet impacts on deep pools: transition from capillary-dominated cavity closure to gas-pressure-dominated closure at higher weber numbers. J. Fluid Mech. 986 (A24).

Liao, Y.-C., Franses, E.I., Basaran, O.A., 2006. Deformation and breakup of a stretching liquid bridge covered with an insoluble surfactant monolayer. Phys. Fluids 18 (2), 022101.

Liao, Y.-C., Subramani, H.J., Franses, E.I., Basaran, O.A., 2004. Effects of soluble surfactants on the deformation and breakup of stretching liquid bridges. Langmuir 20 (23), 9926–9930.

Lohse, D., 2022. Fundamental fluid dynamics challenges in inkjet printing. Annu. Rev. Fluid Mech. 54 (1), 349–382.

Manikantan, H., Squires, T.M., 2020. Surfactant dynamics: hidden variables controlling fluid flows. J. Fluid Mech. 892 (P1).

Martin, G.D., Hoath, S.D., Hutchings, I.M., 2008. Inkjet Printing-the Physics of Manipulating Liquid Jets and Drops. In: Journal of Physics: Conference Series, vol. 105, IOP Publishing, 012001.

Mohammad Karim, A., 2020. Experimental dynamics of newtonian and non-newtonian droplets impacting liquid surface with different rheology. Phys. Fluids 32 (4).

Parmentier, J., Lejeune, S., Maréchal, M., Bourges, F., Genty, D., Terrapon, V., Maréchal, J.-C., Gilet, T., 2019. A drop does not fall in a straight line: a rationale for the width of stalagmites. Proc. R. Soc. A 475 (2231), 20190556.

Prasad, G.V.V., Dhar, P., Samanta, D., 2022. Postponement of dynamic leidenfrost phenomenon during droplet impact of surfactant solutions. Int. J. Heat Mass Transfer 189, 122675.

Quetzeri-Santiago, M.A., Hedegaard, C.L., Castrejón-Pita, J.R., 2019. Additive manufacturing with liquid latex and recycled end-of-life rubber. 3D Print. Addit. Manuf. 6 (3), 149–157.

Roché, M., Aytouna, M., Bonn, D., Kellay, H., 2009. Effect of surface tension variations on the pinch-off behavior of small fluid drops in the presence of surfactants. Phys. Rev. Lett. 103, 264501.

Shin, S., Chergui, J., Juric, D., Kahouadji, L., Matar, O.K., Craster, R.V., 2018. A hybrid interface tracking – level set technique for multiphase flow with soluble surfactant. J. Comput. Phys. 359, 409–435.

Singh, M., Basu, S., Samanta, D., 2025. Non-newtonian fluid droplet impact dynamics on thin liquid films. Phys. Fluids 37 (2).

Sykes, T.C., Cimpeanu, R., Fudge, B.D., Castrejón-Pita, J.R., Castrejón-Pita, A.A., 2023. Droplet impact dynamics on shallow pools. J. Fluid Mech. 970 (A34).

Thoraval, M.-J., Takehara, K., Etoh, T.G., Popinet, S., Ray, P., Josserand, C., Zaleski, S., Thoroddsen, S.T., 2012. von Kármán vortex street within an impacting drop. Phys. Rev. Lett. 108 (26), 264506.

Thoraval, M.-J., Takehara, K., Etoh, T., Thoroddsen, S.T., 2013. Drop impact entrapment of bubble rings. J. Fluid Mech. 724, 234–258.

Thoroddsen, S., 2002. The ejecta sheet generated by the impact of a drop. J. Fluid Mech. 451, 373–381.

Varghese, N., Sykes, T.C., Quetzeri-Santiago, M.A., Castrejón-Pita, A.A., Castrejón-Pita, J.R., 2024. Effect of surfactants on the splashing dynamics of drops impacting smooth substrates. Langmuir 40 (17), 8781–8790.

Worthington, A.M., 1908. A Study of Splashes. Longmans, Green, and Company.

Yu, X., Shao, Y., Teh, K.-Y., Hung, D.L., 2022. Force of droplet impact on thin liquid films. Phys. Fluids 34 (4).